

Electromagnetics Laboratory Report Series

Espoo, May 2006

REPORT 472

IMAGES AND PLANE WAVES

Efficient Field Computation in Electromagnetics and Acoustics

Henrik Wallén

Dissertation for the degree of Doctor of Science in Technology to be presented with due permission of the Department of Electrical and Communications Engineering, for public examination and debate in Auditorium S5 at Helsinki University of Technology (Espoo, Finland), on the 6th of June, 2006, at 12 noon.

Helsinki University of Technology
Department of Electrical and Communications Engineering
Electromagnetics Laboratory

Distribution:

Helsinki University of Technology

Electromagnetics Laboratory

P.O. Box 3000

FI-02015 TKK

Tel. +358-9-451 2264

Fax. +358-9-451 2267

ISBN 951-22-8199-6

ISBN 951-22-8198-8 (PDF)

ISSN 1456-632X

Picaset Oy

Helsinki 2006



HELSINKI UNIVERSITY OF TECHNOLOGY P.O. BOX 1000, FI-02015 TKK http://www.tkk.fi		ABSTRACT OF DOCTORAL DISSERTATION	
Author Henrik Wallén			
Name of the dissertation Images and Plane Waves: Efficient Field Computation in Electromagnetics and Acoustics			
Date of manuscript 10 May 2006		Date of the dissertation 6 June 2006	
<input type="checkbox"/> Monograph		<input checked="" type="checkbox"/> Article dissertation (summary + original articles)	
Department	Department of Electrical and Communications Engineering		
Laboratory	Electromagnetics Laboratory		
Field of research	Electromagnetic Theory, Computational Electromagnetics		
Opponent(s)	Prof. Weng Cho Chew, University of Illinois at Urbana-Champaign, USA		
Supervisor (Instructor)	Prof. Jukka Sarvas, Helsinki University of Technology		
Abstract			
<p>In some simple or canonical problems, analytical solutions offer the most efficient way to compute the electromagnetic or acoustic fields. For arbitrary geometries, efficient numerical methods are needed.</p> <p>This thesis contains new or improved solutions of classical electrostatic problems and some further developments of a variant of the fast multipole method (FMM).</p> <p>In the first part, the electrostatic problems of pairs of both orthogonally intersecting and non-intersecting conducting spheres are solved using Kelvin's image theory. A new efficient method for evaluating the polarizability of two non-intersecting spheres is presented. Novel analytical solutions, and also computationally efficient approximative solutions, are obtained by applying Kelvin's inversion to the electrostatic image solution of a conducting wedge.</p> <p>Integral equation methods are popular for both electrodynamic and acoustic scattering problems. However, to be able to use very large number of unknowns, fast iterative methods, such as the fast multipole method, must be used.</p> <p>In the second part of this thesis, a new broadband variant of the multilevel fast multipole algorithm (MLFMA) is described and used for both acoustic and electromagnetic scattering problems. In particular, the implementation overcomes the low-frequency breakdown of the MLFMA using a combination of the spectral representation of the Green's function and Rokhlin's translation formula.</p>			
Keywords Image theory, Kelvin's inversion, fast multipole method (FMM), sub-wavelength breakdown			
ISBN (printed)	951-22-8199-6	ISSN (printed)	1456-632X
ISBN (pdf)	951-22-8198-8	ISSN (pdf)	
ISBN (others)		Number of pages	37 p. + app. 112 p.
Publisher Electromagnetics Laboratory, Helsinki University of Technology			
Print distribution Electromagnetics Laboratory, Helsinki University of Technology			
<input checked="" type="checkbox"/> The dissertation can be read at http://lib.tkk.fi/Diss/2006/isbn9512281988/			



TEKNISKA HÖGSKOLAN PB 1000, FI-02015 TKK http://www.tkk.fi	SAMMANFATTNING (ABSTRAKT) AV DOKTORSAVHANDLING
Författare Henrik Wallén	
Titel Speglingsteori och planvågor: effektiv beräkning av elektromagnetiska och akustiska fält	
Inlämningsdatum för manuskript 10 maj 2006	Datum för disputation 6 juni 2006
<input type="checkbox"/> Monografi	<input checked="" type="checkbox"/> Sammanläggningsavhandling (sammandrag + separata publikationer)
Avdelning Avdelningen för elektro- och telekommunikationsteknik	Laboratorie Laboratoriet för elektromagnetik
Forskningsområde Elektromagnetisk teori, elektromagnetiska beräkningar	Opponent(er) Prof. Weng Cho Chew, University of Illinois at Urbana-Champaign, USA
Övervakare Prof. Jukka Sarvas, Tekniska högskolan (Handledare)	
Sammanfattning (Abstrakt) <p>I vissa enkla eller kanoniska fall är analytiska lösningar de mest effektiva för beräkandet av elektriska eller akustiska fält. För godtyckliga objekt behövs effektiva numeriska metoder.</p> <p>Denna avhandling innehåller dels nya eller förbättrade lösningar av klassiska elektrostatiske problem och dels en vidareutveckling av en variant av den snabba multipolmetoden (fast multipole method, FMM).</p> <p>I den första delen behandlas elektrostatiske problem med två ledande klot. Lösningen är baserad på Kelvins speglingsteori. En ny effektiv metod för att beräkna polarisabiliteten hos två närliggande klot presenteras. Nya analytiska lösningar, samt numeriskt effektiva approximativa lösningar, fås genom att använda Kelvins inversion på speglingsteori-lösningen för en ledande kil.</p> <p>Metoder baserade på integralekvationer är populära vid lösningen av elektromagnetiska och akustiska spridningsproblem. För att kunna använda väldigt många okända parametrar är det emellertid nödvändigt att använda snabba iterativa lösningsmetoder, så som den snabba multipolmetoden.</p> <p>I den andra delen av avhandlingen presenteras en ny variant av den snabba multipolmetoden med flera nivåer (MLFMA). Metoden utnyttjas för såväl akustiska som elektromagnetiska spridningsproblem. Med hjälp av såväl avklingande som utbredande planvågor lyckas metoden undvika ett sammanbrott vid låga frekvenser, i motsats till traditionella MLFMA-varianter.</p>	
Ämnesord (Nyckelord) Speglingsteori, Kelvins inversion, snabba multipolmetoden (FMM), lågfrekvens-sammanbrott	
ISBN (tryckt) 951-22-8199-6	ISSN (tryckt) 1456-632X
ISBN (pdf) 951-22-8198-8	ISSN (pdf)
ISBN (övriga)	Sidantal 37 s. + bil. 112 s.
Utgivare Laboratoriet för elektromagnetik, Tekniska högskolan	
Distribution av tryckt avhandling Laboratoriet för elektromagnetik, Tekniska högskolan	
<input checked="" type="checkbox"/> Avhandlingen är tillgänglig på nätet http://lib.tkk.fi/Diss/2006/isbn9512281988/	

Contents

Preface	8
List of Publications	9
1 Introduction	10
2 Electrostatics	11
2.1 Background	11
2.2 Formulation	11
2.3 Image Theory	12
2.4 Kelvin's Inversion	15
3 The Fast Multipole Method	17
3.1 Background	17
3.2 FMM and MLFMA	18
3.3 Short Overview of the Algorithm	18
3.4 Plane-Wave Expansions and the Sub-Wavelength Breakdown . .	20
3.5 Broadband MLFMA	23
3.5.1 Error Controllability	25
3.5.2 Computational Complexity	29
4 Summary of the Publications	30
References	32
Errata	37

Preface

This thesis is the result of my research at the Electromagnetics Laboratory of the Helsinki University of Technology. Thanks to the Graduate School of Applied Electromagnetics for funding my research in 2002–2005.

When I started my graduate studies in November 2001, I didn't have a clear research plan. In the beginning, I concentrated on passing the needed courses, and thereafter, I worked on quite varying topics (electromagnetics using differential forms, canonical electrostatic problems and fast multipole methods) in collaboration with all four professors in the laboratory. In the end, to get a thesis with just two different topics instead of three, I decided to exclude the papers on differential forms.¹

I would like to thank my instructors, Prof. Jukka Sarvas, Prof. Keijo Nikoskinen, Prof. Ismo Lindell and Prof. Ari Sihvola, who all have provided guidance and support. Furthermore, I would like to thank Dr. Seppo Järvenpää and Docent Pasi Ylä-Oijala for the collaboration in preparing [P5,P6]. Warm thanks also to the rest of the personnel of the Electromagnetics Laboratory.

Finally, I would also like to thank the pre-examiners, Prof. Karl F. Warnick and Docent Jouni Peltoniemi, whose comments substantially improved the summary part of my thesis.

¹I. V. Lindell and K. H. Wallén, *Journal of Electromagnetic Waves and Applications*, vol. 16, no. 11, pp. 1615–1635, 2002; vol. 18, no. 7, pp. 957–968, 2004; and vol. 18, no. 8, pp. 1045–1056, 2004.

List of Publications

- [P1] I. V. Lindell, K. H. Wallén, and A. H. Sihvola, “Electrostatic image theory for two intersecting conducting spheres,” *Journal of Electromagnetic Waves and Applications*, vol. 17, no. 11, pp. 1643–1660, 2003.
- [P2] H. Wallén and A. Sihvola, “Polarizability of conducting sphere-doublets using series of images,” *Journal of Applied Physics*, vol. 96, no. 4, pp. 2330–2335, Aug. 2004.
- [P3] K. Nikoskinen and H. Wallén, “Application of Kelvin’s inversion to static conducting wedge problems,” *Electromagnetics Laboratory Report Series*, Report 467, Helsinki University of Technology, Espoo, 16 pages, Jan. 2006. Also submitted for publication in *IEE Proc. Science, Measurement & Technology*.
- [P4] H. Wallén and J. Sarvas, “Translation procedures for broadband MLFMA,” *Progress in Electromagnetics Research*, vol. PIER 55, pp. 47–78, 2005.
- [P5] H. Wallén, S. Järvenpää, and P. Ylä-Oijala, “Broadband multilevel fast multipole algorithm for acoustic scattering problems,” *Journal of Computational Acoustics*, 21 pages, accepted for publication, 2006.
- [P6] H. Wallén, S. Järvenpää, P. Ylä-Oijala, and J. Sarvas, “Broadband Müller-MLFMA for electromagnetic scattering by dielectric objects,” *Electromagnetics Laboratory Report Series*, Report 465, Helsinki University of Technology, Espoo, 19 pages, Jan. 2006. Also submitted for publication in *IEEE Transactions on Antennas and Propagation*.

The paper [P1] was the result of a collaboration between the authors, with Prof. Ismo Lindell mainly responsible for the manuscript.

For the paper [P2], I derived the results and wrote most of the manuscript. Prof. Ari Sihvola provided the motivation for the research and insight into the physics behind the polarizability.

The idea behind the paper [P3] came from Prof. Keijo Nikoskinen, but we wrote the manuscript in close co-operation. I computed the numerical results and prepared the figures for the final version of the paper.

I did most of the work behind the paper [P4] and wrote most of the manuscript, with some help and guidance from Prof. Jukka Sarvas. Some initial ideas came from Prof. Jukka Sarvas, but many of the new ideas were mine, and I worked out all the details to get a working algorithm.

In the papers [P5, P6], we accelerated two previously developed iterative solvers using a broadband MLFMA based on [P4]. I developed the basic field representations and translation procedures, but most of the actual code for the solvers was written by Dr. Seppo Järvenpää. I wrote the manuscripts, while Docent Pasi Ylä-Oijala and Prof. Jukka Sarvas provided helpful comments and suggestions.

1 Introduction

Analytical or closed-form solutions, when available, may offer the most efficient way to compute electromagnetic or acoustic fields. However, those solutions sometimes consist of slowly converging infinite series or difficult integrals, and from a computational point of view the path from a closed-form solution to efficient computation of the fields may be surprisingly long. In the general case, the solution is not known in closed form, and we must resort to numerical methods.

This thesis consists of two major topics: closed-form solutions in electrostatics and the fast multipole method.

The first topic, consisting of some introductory material in Section 2 and the papers [P1–P3], is about Kelvin’s inversion and image theory for obtaining new or improved closed-form solutions in electrostatics. In all three cases the solution is expressed using images, but in [P2] the images form an infinite series and in [P3] one image is an infinite line charge. Therefore, the computational aspect is considered in some detail in [P2,P3], to obtain solutions that are also efficient from a numerical point of view.

The second topic, consisting of the introduction in Section 3 and the papers [P4–P6], is about the fast multipole method (FMM) and more specifically how to avoid the sub-wavelength breakdown using a plane-wave expansion of the Green’s function. One key point in the FMM is the efficient representation of fields outside of a source region. Conceptually, this bears some resemblance to image theory, where we seek an image source to efficiently represent the secondary field outside an obstacle.

The main purpose of the summary part of this thesis is to present some introductory material and motivation in Section 2 and Section 3, related to the papers [P1–P3] and [P4–P6], respectively. Sections 3.5.1 and 3.5.2 also contain supplementary material related to the error controllability and computational complexity of the proposed broadband FMM. Finally, Section 4 contains a summary of the results and novel aspects of each paper, and also some additional remarks on the papers.

2 Electrostatics

2.1 Background

The field of electrostatics is old and well documented in several classical textbooks, such as [1–3]. Although most new electromagnetic publications consider time-dependent electromagnetics, such as high-frequency wireless communication, electrostatics is still an important topic.

Regardless of the frequency, if we look at a sufficiently small length scale—smaller than the wavelength—then the fields are essentially static or quasistatic in nature. Therefore, each new electrostatic solution also provides some insight into the local behavior of dynamic electromagnetic fields. The static behavior is especially important if we consider the field singularities near sharp edges and corners.

From a computational electromagnetics point of view, new analytical or closed form solutions are also important—not only as benchmark solutions for testing new computational methods, but also when designing special purpose basis functions or mesh refinements for a specific geometry.

Prof. Ari Sihvola has been very interested in modeling composite materials using mixing theory [4]. A very fundamental concept in this material modeling is the polarizability of the particles or inclusions of a mixture. The polarizability α of an object is defined as the ratio between the induced dipole moment \mathbf{p} and the external static field \mathbf{E}_0 . In general, the polarizability is a linear mapping that can be expressed using a dyadic $\overline{\overline{\alpha}}$ as

$$\mathbf{p} = \overline{\overline{\alpha}} \cdot \mathbf{E}_0. \quad (1)$$

The ongoing quest for accurate values of the polarizability of canonical shapes has, among other things, resulted in one PhD dissertation [5].

The case of two conducting spheres, either intersecting or non-intersecting, seemed like an easy problem when Prof. Ari Sihvola wanted to know the polarizability with high accuracy. However, the solution turned out to be surprisingly complicated and this seemingly easy problem gave rise to the papers [P1, P2].

2.2 Formulation

Consider the following very classical electrostatic problem: Into an empty space with permittivity ϵ_0 , we place a point charge Q at \mathbf{r}_0 near a grounded conducting object that is bounded by the surface S , as shown in Figure 1. The task is to compute the electric field outside the conductor.

As shown in many textbooks [1–3], we can express the electric field \mathbf{E} in terms of a scalar potential as

$$\mathbf{E}(\mathbf{r}) = -\nabla\phi(\mathbf{r}), \quad (2)$$

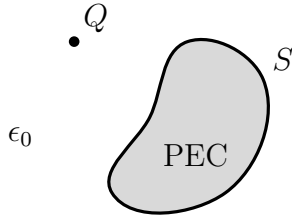


Figure 1: A point charge Q at \mathbf{r}_0 near a conductor bounded by the surface S in an otherwise empty space with permittivity ϵ_0 .

where the potential ϕ satisfies the Poisson equation

$$\nabla^2 \phi(\mathbf{r}) = -\frac{Q}{\epsilon} \delta(\mathbf{r} - \mathbf{r}_0), \quad (3)$$

everywhere outside the conductor. Furthermore, the potential is zero on the conducting surface and at infinity, i.e.,

$$\phi(\mathbf{r}) = 0 \quad \text{when } \mathbf{r} \in S, \quad \text{and} \quad \lim_{r \rightarrow \infty} \phi(\mathbf{r}) = 0. \quad (4)$$

Without the conductor, the solution would be simple. For a point charge Q at \mathbf{r}_0 in free space, the potential is

$$\phi_0(\mathbf{r}) = \frac{Q}{4\pi\epsilon_0 |\mathbf{r} - \mathbf{r}_0|}. \quad (5)$$

Unfortunately, we cannot solve the problem, (3) and (4), in closed form for an arbitrary surface S . We have to either use purely numerical techniques or restrict the shape of the conductor to simple or canonical shapes.

In the papers [P1–P3], we take the latter approach and consider some canonical geometries using image theory and Kelvin’s inversion.

2.3 Image Theory

The image principle, or image theory, offers elegant and efficient solutions for several electrostatic problems. The basic idea is to replace the conductor with an image-charge distribution ϱ_i and express the potential as

$$\phi(\mathbf{r}) = \phi_0(\mathbf{r}) + \phi_i(\mathbf{r}), \quad (6)$$

where ϕ_0 is the potential due to the original point charge in free space (5), and

$$\phi_i(\mathbf{r}) = \int_{\text{spt } \varrho_i} \frac{\varrho_i(\mathbf{r}')}{4\pi\epsilon_0 |\mathbf{r} - \mathbf{r}'|} dV' \quad (7)$$

is the potential due to the image charge in free space. The potential (6) satisfies the Poisson equation (3) outside of the conductor and is zero at infinity for any

image charge q_i located in the region previously occupied by the conductor. Therefore, the remaining problem is to choose the image charge so that the PEC boundary condition is satisfied.

In general, the image charge is not unique, although the potential outside the conductor is. In many simple cases, it is obvious that the simplest image consists of one point charge, as in Figures 2 and 3, or a collection of point charges, as in Figures 4 and 5.

The two most basic cases, which can be found in many classic books, such as [1, 3, 6], are the half-space and the sphere. If we place a point charge Q above a grounded conducting plane, as shown in Figure 2, then we can satisfy the PEC boundary condition by removing the conductor and placing a point charge $-Q$ at the mirror point below the plane.

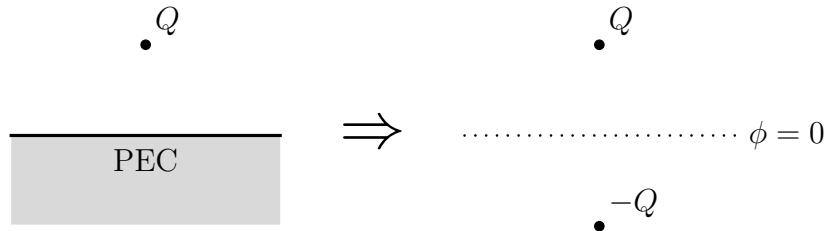


Figure 2: Mirror image principle for a half-space.

For a grounded conducting sphere, Kelvin's image principle [7] states that we can replace the sphere with an image point-charge, as shown in Figure 3, where the charge Q_i and the inverse point d_i are

$$Q_i = -\frac{a}{d}Q \quad \text{and} \quad d_i = \frac{a^2}{d}, \quad (8)$$

if the original point charge Q is placed at the distance d from the center of a sphere with radius a .

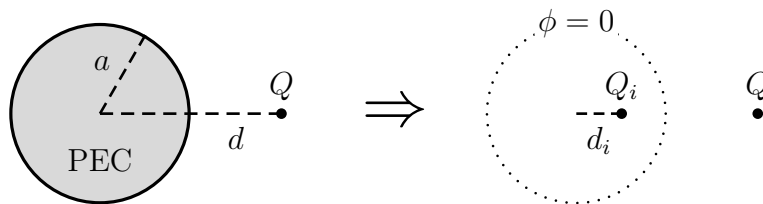


Figure 3: Kelvin's image principle for a sphere.

These two basic cases can be combined in different ways. For instance, for a conducting corner whose angle is π/n , with $n = 2, 3, \dots$, the image consists of $2n - 1$ point charges that can be found using multiple reflections, as in Figure 4 for the case $n = 3$. As a second example, the combination of a sphere and a half-space gives us the solution for the geometry in Figure 5.

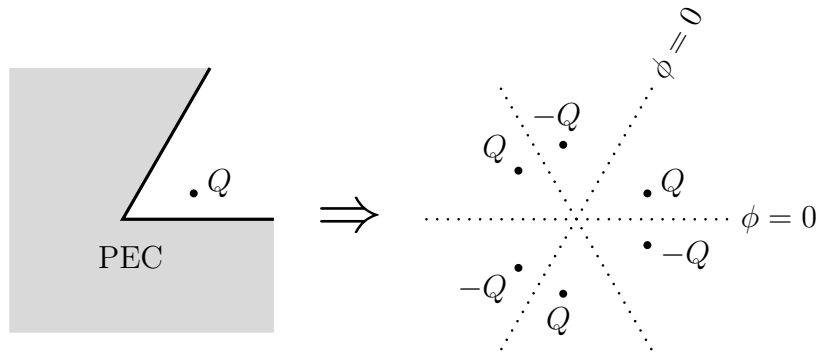


Figure 4: Image solution for a $\pi/3$ corner.

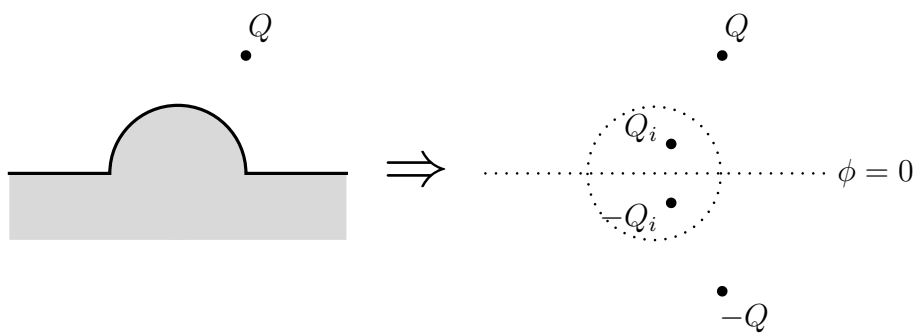


Figure 5: Image solution for a half-space with a half-spherical boss.

A system of two spheres can also be considered using Kelvin's image principle: First we use the image principle to compensate for the original charge, then we use the image principle again to compensate for the first images in the opposite spheres, and so on. If the spheres intersect at an angle π/n , with $n = 2, 3, \dots$, we get $2n - 1$ images, similarly as for a π/n corner. This case is considered in [P1] for two orthogonally intersecting spheres. If the two spheres are separated, we get infinite series of images. This latter case is in turn considered in [P2].

2.4 Kelvin's Inversion

Kelvin's inversion [8] is a space transformation that maps the inside of a sphere to the outside and vice versa. If we, for simplicity, choose the origin of the coordinate-system to coincide with the center of the inversion sphere, then the transformation $\mathbf{r} \rightarrow \mathbf{K}(\mathbf{r})$ is

$$\mathbf{K}(\mathbf{r}) = \frac{a^2}{r^2} \mathbf{r}, \quad (9)$$

where a is the radius of the inversion sphere and we use the notation $r = |\mathbf{r}|$.

Geometrically, the inversion maps spheres and planes not intersecting the inversion origin into spheres, while spheres and planes intersecting the inversion origin are mapped into planes. Furthermore, the inversion is a conformal mapping, that is, any angle is mapped into an equal angle [10].

If we apply the transformation (9) to the Poisson equation (3), we get a new solution ϕ_K satisfying

$$\nabla^2 \phi_K(\mathbf{r}) = \nabla^2 \left(\frac{r_0}{r} \phi(\mathbf{K}(\mathbf{r})) \right) = -\frac{Q}{\epsilon_0} \delta(\mathbf{r} - \mathbf{K}(\mathbf{r}_0)). \quad (10)$$

The transformation also preserves the PEC boundary condition,

$$\phi = 0 \quad \text{on } S \quad \Leftrightarrow \quad \phi_K = 0 \quad \text{on } S_K, \quad (11)$$

where S_K is the transformed boundary. Therefore, if we know the potential ϕ due to a point charge Q at \mathbf{r}_0 near a conducting surface S , then we get the solution ϕ_K due to the shifted point charge Q at $\mathbf{K}(\mathbf{r}_0)$ near the transformed boundary S_K using Kelvin's inversion.

Kelvin's inversion and Kelvin's image principle for a sphere are closely related. In fact, we could derive the image principle for a sphere by applying the inversion on the half-space solution of Figure 2, as sketched in Figure 6. The potential before inversion can be expressed using one mirror-image charge. After transforming the potential using (10), we can identify the same Kelvin image inside the sphere as in Figure 3.

In [P3], we start from the image theory for a conducting wedge [11] and apply Kelvin's inversion on the resulting potential. In this way we get the potential due to a point charge near a conducting object bounded by two spherical surfaces intersecting in any angle. Two examples of the obtained geometries are shown in Figure 7.

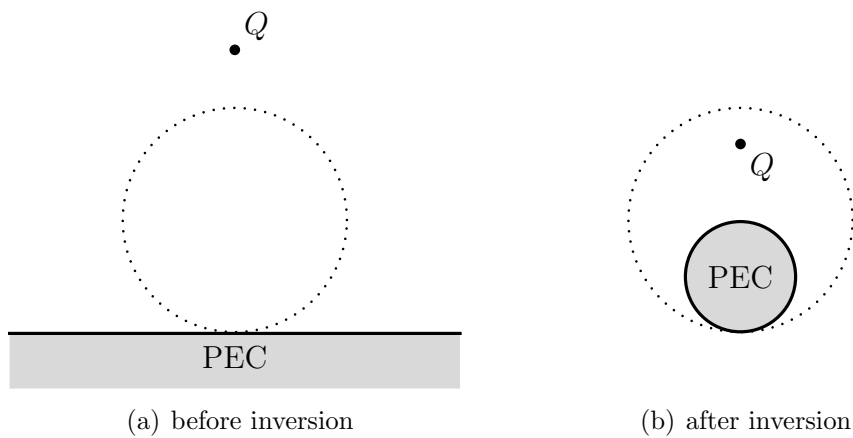


Figure 6: Kelvin's image principle using Kelvin's inversion. The dotted circle shows the location of the inversion sphere.

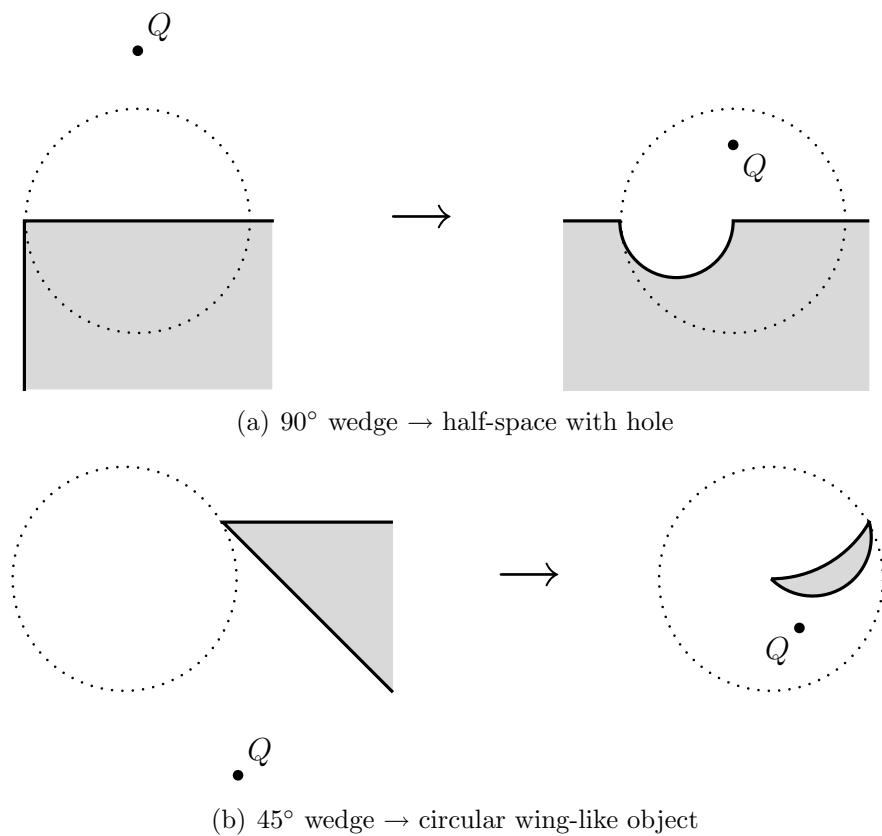


Figure 7: Kelvin's inversion of a conducting wedge. The potential in these two example geometries are considered in [P3].

3 The Fast Multipole Method

3.1 Background

Most of the general purpose methods in computational electromagnetics can be divided into two categories: methods based on differential equations and integral equations.

In the differential equation methods—such as the finite element method (FEM) [12–14], and the finite-difference time-domain method (FD-TD) [15, 16]—the whole computational domain is discretized and the fields are used as unknowns. This leads to a sparse system matrix (FEM) or even to no system matrix at all (FD-TD). However, the needed number of unknowns is typically large. Furthermore, for scattering and antenna applications the computational domain must be artificially truncated.

In the method of moments (MoM)² or integral equation methods [17–20] (equivalent) sources are used as unknowns instead of the fields. This leads to a full system matrix, and the elements of the system matrix must be computed from (weakly) singular integrals. However, especially for surface integral equations, the needed number of unknowns is typically much smaller than for a comparable differential equation solution.

Surface integral equation methods are well suited for scattering and radiation problems involving conducting and piecewise homogeneous dielectric structures, especially if we are interested only in one or a few frequencies. In many other cases, some other method may be preferable. My colleagues at the TKK Electromagnetics Laboratory have been extensively researching the surface integral equation methods, resulting in several important contributions to the field, such as [21–24].

The major bottleneck in integral equation methods is the full system matrix. For N unknowns, the memory consumption is $\mathcal{O}(N^2)$ to store the system matrix and $\mathcal{O}(N^3)$ to solve the matrix equation using a direct solver. Iterative solvers lowers the computational cost to $\mathcal{O}(N^2)$ per iteration, but this is still too much for very large N . To be able to use very large numbers of unknowns, we need to use an iterative fast solver, where the needed matrix-vector multiplications with the system matrix are performed efficiently, without assembling the actual system matrix. Popular fast solvers include the FFT-based method, the adaptive integral method and the fast multipole method (FMM)—see, for instance [14, Ch. 14], for a nice overview and comparison.

Many FMM-solvers suffer from two kinds of sub-wavelength breakdowns: neither the underlying integral equation formulation nor the (high-frequency) FMM works flawlessly when the discretization is very fine compared with the wavelength. Recently, my colleagues have invented new surface integral equation formulations that overcome the first sub-wavelength breakdown [24, 25],

²Harrington’s MoM [17] is actually a very general concept, but in electrical engineering the term usually refers to integral equation methods.

and the particular contribution of this thesis is a new variant of the FMM that overcomes the second sub-wavelength breakdown in a fairly straightforward manner using evanescent plane-wave expansions.

3.2 FMM and MLFMA

The original fast multipole method (static FMM) was presented for the Laplace equation in two and three dimensions by Greengard and Rokhlin [26,27]. One early application in electrical engineering was to speed up the capacitance extraction of conducting structures [28,29].

Later, Rokhlin developed a version of the FMM (HF-FMM) that is suitable for the Helmholtz equation at high frequencies [30–32]. One-level implementations of the algorithm was presented in 2-D [33] and 3-D [34,35], and shortly thereafter multilevel versions in 3-D [36–40]. Meanwhile, the mathematical theory of the FMM and its error analysis was studied in [41,42]. Today, the multilevel fast multipole algorithm (MLFMA) for computational electromagnetics, by Chew et al. [37,38,43,44], can be considered well established.

The FMM, in its various incarnations, can be used for gravitational N-body problems and, in particular, for solving various electrostatic, acoustic and electrodynamic problems with integral equation methods.

In an N-body problem, a direct computation of the interactions between N particles has a computational cost of $\mathcal{O}(N^2)$. Similarly, for the iterative solution of an integral equation that is discretized using N basis functions, the computational cost of each iteration is also $\mathcal{O}(N^2)$, since the interactions between all N basis functions need to be computed. For the Laplace equation, the static FMM lowers the cost to $\mathcal{O}(N)$. For the Helmholtz equation, the HF-FMM using one level lowers the cost to $\mathcal{O}(N^{3/2})$ and the MLFMA further to $\mathcal{O}(N \log N)$.

3.3 Short Overview of the Algorithm

To illustrate the basic concepts of the FMM and MLFMA, let us consider the following N-body problem. Assume that we have N point sources q_n at \mathbf{r}_n , for $n = 1, \dots, N$. The task is to compute the scalar field F_m at each point source due to all other point sources, given by

$$F_m = F(\mathbf{r}_m) = \sum_{\substack{n=1 \\ n \neq m}}^N G(\mathbf{r}_m - \mathbf{r}_n) q_n, \quad \text{for } m = 1, \dots, N, \quad (12)$$

where G is the Green's function

$$G(\mathbf{r} - \mathbf{r}') = \frac{e^{ik|\mathbf{r}-\mathbf{r}'|}}{4\pi|\mathbf{r} - \mathbf{r}'|} \quad (13)$$

that satisfies the Helmholtz equation $(\nabla^2 + k^2)G(\mathbf{r} - \mathbf{r}') = -\delta(\mathbf{r} - \mathbf{r}')$.

A direct computation of all the $N(N - 1)$ interactions becomes expensive if N is large enough. The basic idea of the FMM is to group the sources and compute most of the interactions between the groups instead of directly between the sources.

To get an efficient implementation, the key building blocks are the field representations (both for the field outside a group due to the sources inside the group and for the local field inside a group due to sources outside) and the translation procedures between the different representations. The implementation details of the representations and translations are different in the static case and the high-frequency case, but the basic algorithm consists of the following steps.

Preprocessing

To begin, we enclose all point sources in a large cube at level 0. Then, we recursively subdivide the cube into eight sub-cubes, or children cubes, at level 1, 2, \dots , l_{\max} . Each cube is then either a childless cube containing a modest number of point sources, say between 10 and 100, or else a parent cube with one to eight children cubes. We store all (non-empty) cubes in a tree.

Two cubes are *nearby* if they are at the same level and share at least one boundary point (a cube is then nearby itself). Two cubes are *well separated* if they are at the same level and not nearby each other. The *interaction list* of a cube consists of all well-separated cubes that are contained in nearby cubes at the parent level. It follows that the interaction list of a cube can contain up to $6^3 - 3^3 = 189$ cubes.

Aggregation

In the first, up-tree³ pass, we recursively compute and store the outgoing representation for each cube at level 2, \dots , l_{\max} .

For a childless cube, we compute the outgoing representation from the sources contained in the cube. For a parent cube, we combine the outgoing representations from its children cubes.

Translation and disaggregation

In the second, down-tree pass, we translate the fields from outgoing to incoming representations at the coarsest possible level, and also distribute the incoming field from parent cubes to their children cubes. By traversing the tree in depth-first order, we do not need to store more than one incoming representation per level.

At levels 0 and 1 there are no well-separated cubes, and thus the incoming representation for each cube is zero. For a cube at level 2, we get the incoming representation by translating the outgoing representation

³A computer science tree is typically drawn with the root at the top (the level 0 cube) and the leaves at the bottom (the level l_{\max} cubes).

from each cube in the interaction list into an incoming representation in the cube under consideration. For a cube at level $3, \dots, l_{\max}$, we distribute the incoming representation from the parent cube and add the representation translated from the cubes in the interaction list.

Finally, for a cube at level l_{\max} , we have an incoming representation of the field due to all sources in well-separated cubes. Then, we compute the field F_m at each point in the cube using this incoming representation, and add the field due to the sources in nearby cubes using a direct computation.

As a simple example, let us assume that we have $N = 20000$ point sources that are uniformly distributed in a cube. Then, four levels gives us $8^3 = 512$ cubes at level $l_{\max} = 3$, with about 39 point sources in each cube. The up-tree pass is illustrated in Figure 8 and the down-tree pass in Figures 9 and 10.

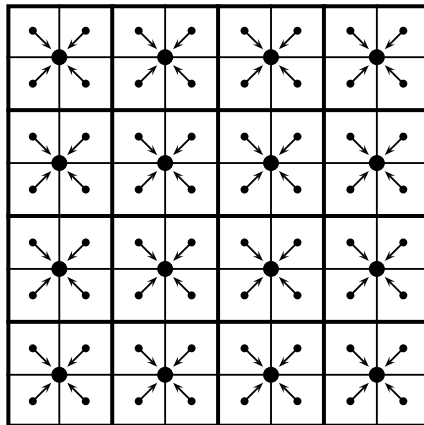


Figure 8: Aggregation from level 3 (small cubes) to level 2 (large cubes). For each cube at level 2, we combine the outgoing representations from its children cubes. For the cubes at level 3, we compute the outgoing representations from the point sources.

3.4 Plane-Wave Expansions and the Sub-Wavelength Breakdown

In the static FMM ($k = 0$), the fields are represented using multipole expansions. The HF-FMM and MLFMA are instead based on a plane-wave expansion of the Green's function (13) due to Rokhlin [31, 32]. This plane-wave expansion can be written in the general form

$$G(\mathbf{D} + \mathbf{d}) = \frac{e^{ik|\mathbf{D}+\mathbf{d}|}}{4\pi|\mathbf{D} + \mathbf{d}|} \approx \int_{S^2} T(\mathbf{k}, \mathbf{D}) e^{i\mathbf{k}\cdot\mathbf{d}} d\hat{\mathbf{k}}, \quad D > d, \quad (14)$$

where the integration is with respect to $\hat{\mathbf{k}}$ over the unit sphere, $\mathbf{k} = k\hat{\mathbf{k}}$, and $T(\mathbf{k}, \mathbf{D})$ is the translation function. Written out explicitly, Rokhlin's

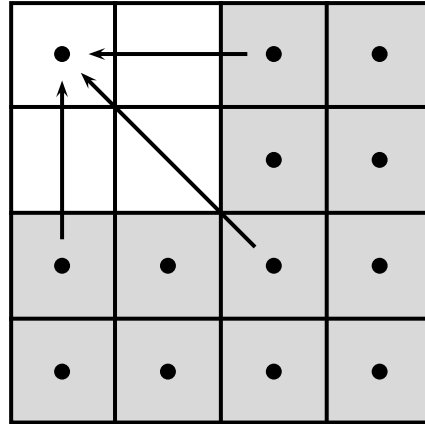


Figure 9: Translation on level 2 from all the gray cubes to the white cube in the upper left corner.

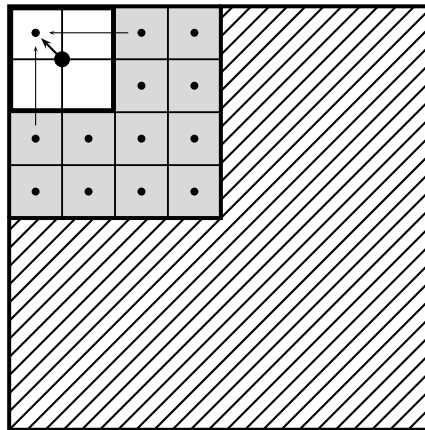


Figure 10: Translation on level 3 from all the gray cubes to the white cube in the upper left corner. The contribution due to the cubes in the hatched region is distributed from the parent cube.

translation formula is

$$G(\mathbf{D} + \mathbf{d}) \approx \int_{-\pi}^{\pi} \int_0^{\pi} T_L(\theta, \varphi) e^{i\mathbf{k}(\theta, \varphi) \cdot \mathbf{d}} \sin \theta \, d\theta \, d\varphi, \quad D > d, \quad (15)$$

where the wave-vector \mathbf{k} and the translation function $T = T_L$ are expressed as functions of the spherical coordinates θ and φ as

$$\mathbf{k}(\theta, \varphi) = k((\hat{\mathbf{x}} \cos \varphi + \hat{\mathbf{y}} \sin \varphi) \sin \theta + \hat{\mathbf{z}} \cos \theta) \quad \text{and} \quad (16)$$

$$T_L(\theta, \varphi) = \frac{ik}{(4\pi)^2} \sum_{n=0}^L i^n (2n+1) h_n^{(1)}(kD) P_n \left(\frac{\mathbf{k}(\theta, \varphi) \cdot \mathbf{D}}{kD} \right). \quad (17)$$

Here, $h_n^{(1)}$ is the spherical Hankel function of the first kind and degree n , and P_n is the Legendre polynomial of degree n .

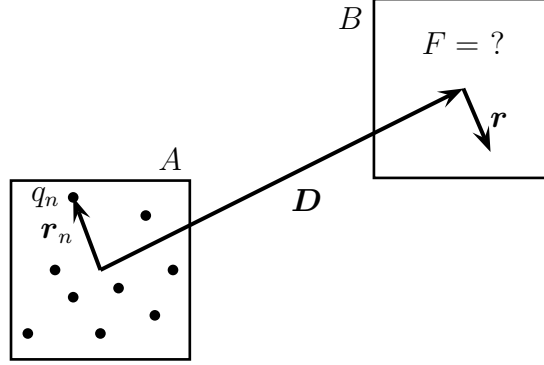


Figure 11: Field inside the cube B due to point sources in the cube A .

Consider the field $F(\mathbf{D} + \mathbf{r})$ inside the cube B , centered at \mathbf{D} , due to the point sources inside the well-separated cube A , centered at the origin, as shown in Figure 11. Using (14), we get the plane-wave expansion

$$\begin{aligned} F(\mathbf{D} + \mathbf{r}) &= \sum_n G(\mathbf{D} + \mathbf{r} - \mathbf{r}_n) q_n \\ &= \int_{S^2} \left(\sum_n q_n e^{-i\mathbf{k} \cdot \mathbf{r}_n} \right) T(\mathbf{k}, \mathbf{D}) e^{i\mathbf{k} \cdot \mathbf{r}} \, d\hat{\mathbf{k}} \\ &= \int_{S^2} v(\mathbf{k}) e^{i\mathbf{k} \cdot \mathbf{r}} \, d\hat{\mathbf{k}}, \end{aligned} \quad (18)$$

where

$$v(\mathbf{k}) = u_{\infty}(\mathbf{k}) T(\mathbf{k}, \mathbf{D}) \quad (19)$$

is the incoming-wave pattern of the plane-wave expansion, and

$$u_{\infty}(\mathbf{k}) = \sum_n q_n e^{-i\mathbf{k} \cdot \mathbf{r}_n} \quad (20)$$

is the radiation pattern due to the point sources in the cube A . The summation in (20) is over all point sources that are inside the cube.

The basic strategy to implement the MLFMA, is to use samples of the radiation patterns to represent outgoing fields and samples of the incoming-wave patterns to represent incoming or local fields. A translation from an outgoing representation into an incoming one is given by the point-wise multiplication in (19) for each sample point. A shift of origin for a radiation or incoming-wave pattern is a point-wise multiplication with $e^{i\mathbf{k}\cdot\mathbf{p}}$ for each sample point, with \mathbf{p} being a vector from the old origin to the new one. In addition, since the needed sample rates are different for different levels, we also need interpolation and antinterpolation procedures between the sample points at adjacent levels.

When $k \rightarrow 0$, the radiation pattern (20) degenerates into a constant,

$$u_\infty \rightarrow \sum_n q_n. \quad (21)$$

Therefore, without even looking at the expression for the translation function $T(\mathbf{k}, \mathbf{D})$, we can conclude that *the radiation pattern does not contain enough information to represent the outgoing field for a cube that is too small compared with the wavelength*. This is the well-known sub-wavelength or low-frequency breakdown of the HF-FMM and MLFMA.

Another way to explain the sub-wavelength breakdown is to look at the the translation function (17). The order L must be large enough to get good accuracy, but the sum is divergent as $L \rightarrow \infty$. The spherical Hankel function $h_n^{(1)}(kD)$ grows exponentially with increasing degree when the degree n is larger than the argument kD . Therefore, L cannot be much larger than kD .

In practice, the side length of the cubes must be around one quarter of a wavelength or larger to ensure acceptable accuracy.

3.5 Broadband MLFMA

To overcome the sub-wavelength breakdown, and get a broadband algorithm that works for all frequencies or cube sizes, we have two basic options. One possibility is to combine the (high-frequency) MLFMA with a low-frequency one based on dynamic multipole-expansions as in [45–47]. The other option is to use a low-frequency stable plane-wave expansion, instead of Rokhlin’s translation formula, to get a broadband algorithm as in [48–50].

To use plane-wave expansions in the sub-wavelength scale we need to include evanescent waves (with complex \mathbf{k}) in addition to ordinary propagating waves. The wave vector must satisfy $\mathbf{k} \cdot \mathbf{k} = k^2$, so that the plane waves satisfy the Helmholtz equation, but if the wave vector is complex, it can remain non-zero when the frequency goes to zero ($k \rightarrow 0$). The approach in [48, 49] is based on the spectral representation of the Green’s function, while the approach in [50] is based on a more heuristic way to include evanescent waves.

The spectral representation of the Green’s function, which seems to be the most promising low-frequency stable plane-wave expansion, can be written in

the form (14) as

$$G(\mathbf{D} + \mathbf{d}) = \int_{-\pi}^{\pi} \int_{\Gamma} T(\mathbf{k}, \mathbf{D}) e^{i\mathbf{k} \cdot \mathbf{d}} \sin \theta \, d\theta \, d\varphi, \quad \widehat{\mathbf{z}} \cdot (\mathbf{D} + \mathbf{d}) > 0, \quad (22)$$

where wave vector $\mathbf{k} = \mathbf{k}(\theta, \varphi)$ is given by (16), the path $\Gamma = \Gamma_p + \Gamma_e$ in the complex θ -plane is given in Figure 12, and the translation function is

$$T(\mathbf{k}, \mathbf{D}) = T(\theta, \varphi) = \frac{ik}{8\pi^2} e^{i\mathbf{k}(\theta, \varphi) \cdot \mathbf{D}}. \quad (23)$$

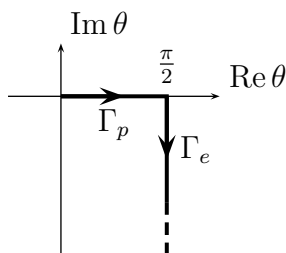


Figure 12: The integration path $\Gamma = \Gamma_p + \Gamma_e$ in the complex plane.

The spectral representation of the Green's function can be split in two parts by considering the integration paths Γ_p and Γ_e separately. For the *propagating part*, corresponding to Γ_p , the wave-vector \mathbf{k} is real⁴ and the integration is over the upper half ($z > 0$) of the unit sphere with respect to $\widehat{\mathbf{k}}(\theta, \varphi)$. For the *evanescent part*, corresponding to Γ_e , \mathbf{k} is complex, that is, the representation is based on evanescent plane-waves.

The spectral representation (22) is in principle exact for any k including $k \rightarrow 0$, but the representation is direction dependent. Moreover, we need to efficiently evaluate a semi-infinite integral in the complex θ -plane.

For the propagating part, we embed the direction dependency into the translation function so that we can use exactly the same propagating representations as with Rokhlin's translation formula. This makes the combination of the spectral representation and Rokhlin's translation formula nearly trivial, but the downside is that we get a non-smooth translation function, leading to somewhat complicated translation procedures.

For the evanescent part, we need six expansions, but we can use a highly efficient generalized Gaussian quadrature rule for the semi-infinite integral in $\sigma = -ik \cos \theta$.

The fundamental translation procedures are explained in detail in [P4], and actual broadband MLFMA implementations for acoustic and electromagnetic scattering are presented in [P5, P6], using a combination of the spectral

⁴Here we assume that the wave-number k is real, i.e., that the surrounding free space is lossless.

representation and Rokhlin’s translation formula. Two outstanding questions regarding the error controllability and the computational complexity are considered in some details in the following to supplement the findings reported in [P4–P6].

3.5.1 Error Controllability

The error controllability of the translation procedures, using the spectral representation of the Green’s function, is claimed to be good for up to at least four digits accuracy in [P4]. However, the error controllability seems to be slightly worse in the actual implementations in [P5, P6]. So, what is causing this inaccuracy and is it a serious problem?

- The error controllability of the propagating part is excellent—by adjusting the sample rates or degrees as described in [P4] the error can be made as small as wanted.
- The new quadrature rules that we use for the evanescent part is accurate and error-controllable, which means that there cannot be any problems with the outer-to-inner translations of the evanescent part, at least when considered separately.
- Therefore, any unexpected inaccuracy must be due to the interpolations and antinterpolations of the evanescent part.

To get some numbers to support this conclusion, consider a similar source cube as in the benchmark case in [P4], shown in Figure 13. The cube is centered at the origin and its side length is $a = 2$. The cube contains 100 point sources $q_n = 1$ at the points \mathbf{r}_n , whose Cartesian coordinates are

$$\begin{cases} x_n = z_n = \frac{(n-1) \% 10}{5} - \frac{9}{10} \\ y_n = \frac{\lfloor (n-1)/10 \rfloor}{5} - \frac{9}{10} \end{cases} \quad (24)$$

for $n = 1, 2, \dots, 100$, where $\%$ denotes the modulus or remainder after integer division and $\lfloor \cdot \rfloor$ denotes the floor function.

Using the same level numbering as in [P4, P5], we choose the wave-number k so that $ka = 2^\ell \pi$ if the initial level number is ℓ . This means that the side length a is $2^{\ell-1}$ wavelengths.⁵ As described in [P4], the evanescent radiation pattern for this cube is

$$F_\infty^e(\sigma, \varphi) = \sum_{n=1}^{100} e^{-i\mathbf{k}(\sigma, \varphi) \cdot \mathbf{r}_n} q_n, \quad (25)$$

⁵Note that the level numbering using the symbol ℓ , used in the following, is the same as in [P4, P5] but different from the one using l in Section 3.3.

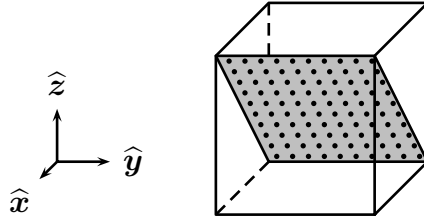


Figure 13: Geometry of the source cube. The cube, at level ℓ , is centered at the origin and its side length is 2. The shaded source plane contains 10×10 point sources of unit amplitude.

where $\sigma = -ik \cos \theta$.

Now, the numerical test is the following. First, we compute the sample matrix [P4, Eq. (49)] of the evanescent radiation pattern (25). Then, we perform successive aggregation steps, exactly as described in [P4], to get the sample-matrices of ever larger parental cubes containing only this single initial cube. We shift the origin so that the original level ℓ cube is in the same corner of all parent cubes, as shown in Figure 14. Finally, we compute the exact sample matrix for the parent cubes, directly from the sources, and use the relative L_2 -error of the aggregated sample matrix as an error estimate.

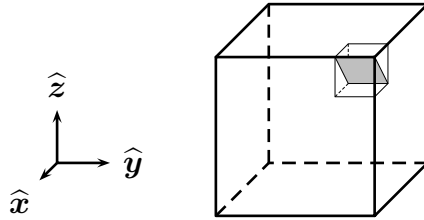


Figure 14: Geometry at level $\ell + 2$, that is, after two interpolations and shifts of origin. The original level ℓ cube and the sources are in one corner of the level $\ell + 2$ cube.

The result of this numerical test is shown in Table 1 for two digits target accuracy and in Table 2 for four digits target accuracy. The errors in the sample matrices are mainly due to the interpolation in the complex θ -variable, since the shifts of origin and interpolations in φ are accurate. Although we cannot draw too sharp conclusions based on this test, the results clearly suggest three things:

1. The accuracy in *one* interpolation is good. (This is also evident from the numerical test in [P4], using only two levels.)
2. The accuracy degrades somewhat with increasing number of interpolations, that is with increasing number of levels.
3. The accuracy is better for lower levels, that is, for cubes that are small compared with the wavelength. This can also be intuitively expected,

	$\ell + 1$	$\ell + 2$	$\ell + 3$	$\ell + 4$	$\ell + 5$	$\ell + 6$
-2	3.32e-04					
-3	8.76e-05	9.29e-04				
-4	5.26e-05	5.78e-04	9.42e-04			
-5	1.23e-05	8.53e-04	1.20e-03	1.59e-03		
-6	5.11e-06	5.86e-04	1.54e-03	2.14e-03	2.52e-03	
-7	4.74e-06	2.46e-04	9.38e-04	2.01e-03	2.87e-03	3.31e-03
-8	4.72e-06	7.38e-05	3.71e-04	1.13e-03	2.30e-03	3.34e-03
-9	4.72e-06	1.91e-05	1.11e-04	4.37e-04	1.24e-03	2.48e-03
-10	4.72e-06	5.21e-06	3.15e-05	1.36e-04	4.81e-04	1.31e-03
-11	4.72e-06	4.85e-06	1.57e-05	5.15e-05	1.65e-04	5.23e-04
-12	4.72e-06	4.92e-06	1.43e-05	3.78e-05	7.96e-05	2.01e-04
-13	4.72e-06	4.94e-06	1.41e-05	3.62e-05	6.37e-05	1.16e-04
-14	4.72e-06	4.95e-06	1.41e-05	3.59e-05	6.10e-05	9.85e-05
-15	4.72e-06	4.95e-06	1.41e-05	3.58e-05	6.04e-05	9.45e-05
-16	4.72e-06	4.95e-06	1.41e-05	3.58e-05	6.03e-05	9.36e-05
-17	4.72e-06	4.95e-06	1.41e-05	3.58e-05	6.03e-05	9.34e-05

Table 1: Relative L_2 -errors in the sample matrices of the evanescent radiation pattern at levels $\ell + 1, \dots, \ell + 6$, for different starting levels $\ell = -2, \dots, -17$. The target accuracy is $d_0 = 2$, and thus we do not need to use the evanescent part for levels $\ell \geq 0$.

	$\ell + 1$	$\ell + 2$	$\ell + 3$	$\ell + 4$	$\ell + 5$	$\ell + 6$
0	1.15e-05					
-1	1.51e-05	5.31e-06				
-2	4.89e-05	2.65e-05	1.65e-05			
-3	7.04e-05	3.58e-05	4.40e-05	5.02e-05		
-4	2.08e-05	1.83e-04	5.02e-05	1.46e-04	2.14e-04	
-5	4.28e-06	2.46e-04	1.38e-04	2.02e-04	3.97e-04	7.11e-04
-6	7.84e-07	1.51e-04	1.86e-04	1.61e-04	1.80e-04	3.82e-04
-7	8.35e-08	6.86e-05	1.40e-04	1.93e-04	2.16e-04	2.54e-04
-8	4.23e-08	2.40e-05	7.15e-05	1.45e-04	2.15e-04	2.47e-04
-9	4.13e-08	6.76e-06	2.52e-05	7.19e-05	1.50e-04	2.25e-04
-10	4.13e-08	1.75e-06	7.09e-06	2.49e-05	7.19e-05	1.51e-04
-11	4.13e-08	4.39e-07	1.83e-06	6.96e-06	2.46e-05	7.16e-05
-12	4.13e-08	1.08e-07	4.61e-07	1.79e-06	6.84e-06	2.43e-05
-13	4.13e-08	2.63e-08	1.15e-07	4.51e-07	1.76e-06	6.76e-06
-14	4.13e-08	1.95e-08	3.43e-08	1.13e-07	4.39e-07	1.73e-06
-15	4.13e-08	1.99e-08	3.28e-08	6.57e-08	1.64e-07	4.36e-07
-16	4.13e-08	2.01e-08	3.28e-08	6.58e-08	1.66e-07	2.87e-07
-17	4.13e-08	2.01e-08	3.28e-08	6.59e-08	1.67e-07	2.92e-07

Table 2: As Table 1, but using $d_0 = 4$ digits target accuracy and levels up to $\ell = 1$.

since the situation is (quasi)static for small cubes, while the dynamic properties dominate for large cubes. Hence, there is a transition region, say at levels $\ell = -4, \dots, 1$, where the properties of the evanescent radiation pattern changes significantly. This is also, at least approximately, the region where the interpolation errors are largest.

To understand the reason for the error accumulation with increasing levels, it is illuminating to look at the condition number (defined as the the largest singular value divided by the smallest singular value) of the interpolation matrices E^ℓ , computed as in [P4, Section 3.2.2]. Table 3 shows the sizes and condition numbers of the interpolation matrices for two and four digits target accuracy. The condition number increases with increasing number of samples in the complex θ -variable, and the interpolation eventually becomes unstable. Using the present interpolation scheme, it is not useful to increase the target accuracy beyond four digits.

ℓ	$d_0 = 2$		$d_0 = 4$	
	size	cond	size	cond
0			7×9	2.88e+02
-1			9×10	1.06e+05
-2	5×5	5.01e+02	10×11	1.26e+06
-3	5×6	7.81e+01	11×11	6.53e+08
-4	6×6	8.92e+03	11×11	7.18e+08
-5	6×6	8.96e+03	11×11	7.30e+08
-6	6×6	8.96e+03	11×11	7.30e+08
-7	6×6	8.96e+03	11×11	7.30e+08

Table 3: Size and condition number of the interpolation matrices E^ℓ at different levels ℓ and $d_0 = 2, 4$ digits target accuracy.

In conclusion, the weakest point in the error controllability is the interpolation in the complex θ -variable. The errors are largest in the transition region at levels $-4 \leq \ell \leq 1$, that is when the side lengths a of the cubes are $\lambda/32 \leq a \leq \lambda$, with λ being the wavelength.

However, for many practical purposes it seems sufficient to obtain one or even a few percents accuracy in the MLFMA, and then the above inaccuracy should not be a significant problem. The actual computations in [P5, P6] also suggest that the accuracy is sufficient, at least for practical accuracy demands.

Note also that in the usual (high-frequency) MLFMA, the accuracy is quite limited if we insist on using cubes whose side lengths are somewhat smaller than the wavelength, as is usually done. If the smallest cubes have side lengths $\lambda/4 \leq a \leq \lambda/2$, which seems to be close to the current state-of-art, then the maximum obtainable accuracy is approximately one percent (or at least not much better) when using Rokhlin's translation formula.

Finally, there is also one additional source of inaccuracy in our point-based MLFMA implementation in [P5, P6] that is not dependent on the actual trans-

lation procedures: Each interaction between two basis functions must be computed either directly or using the MLFMA, but partial interactions are inevitably computed in a point-based MLFMA. These partial interactions are approximately computed using the MLFMA, but the correction terms are computed using the exact Green’s function. If the cubes are too small compared with the basis functions, these correction terms actually increase the memory consumption and the additional errors could also be significant—especially since the errors are in near interaction terms of the system matrix.

3.5.2 Computational Complexity

The computational complexity of the proposed broadband MLFMA is dependent both on the discretization, i.e., the number of unknowns, and on the size of the computational domain in terms of wavelengths. We can, however, easily get rough estimates of the computational complexity in the high-frequency case and in the quasistatic limit.

For the high-frequency case, assume that the discretization is fixed with respect to the wavelength and that we increase the number of unknowns N , so that we have a fixed (small) number of unknowns in each childless cube at level $\ell = 0$. Then, we essentially use the FFT-based MLFMA of [51] without any evanescent representations. In that case, the computational complexity is in theory slightly worse than in the MLFMA by Chew et al. [37,38,43], since the interpolations using FFT are asymptotically less efficient than sparse Lagrangian interpolations. However, as shown in [51], the FFT-based implementation can be more efficient for cubes whose side lengths are up to 16 wavelengths. The memory consumption should also be smaller in the FFT-based MLFMA, since we can use smaller sample rates for the radiation patterns and incoming wave patterns.

For the quasistatic limit, we assume that all cubes are small compared with the wavelength. Then, we can ignore the propagating part and assume that we use the same sample rate to represent the evanescent part for each cube. Furthermore, if we again assume that we have a fixed (small) number of unknowns in each childless cube, then we get $\mathcal{O}(N)$ cubes and both the memory consumption and computational cost is fixed for each cube. Therefore, both the computational cost and memory consumption are asymptotically $\mathcal{O}(N)$ as in the static FMM. In the static FMM, the fields are represented using multipole series of degree p , needing $(p + 1)^2$ coefficients. For two digits accuracy we should choose $p = 7$ or maybe $p = 6$, which gives 64 or 49 coefficients to store one expansion. As listed in [P4, Table 2], we need $6 \times 10 = 60$ samples to store one evanescent radiation pattern (and $6 \times 18 = 108$ samples to perform the outer-to-inner translation). We need 6 evanescent representations to cover all translation directions, but it is not necessary to consider all directions at the same time. To reduce the memory consumption, we could consider one of the six directions at a time, and reuse the same memory for all six radiation patterns for each cube. Then, our memory consumption could optimally be

quite close to the static FMM in the quasistatic limit, aiming at two digits accuracy.

Our present implementations in [P5, P6] are unfortunately not as optimal as the above theoretical rough estimate. However, looking at [P5, Table 4] and comparing the adaptive subdivision cases, we can observe that both the memory consumption and the execution time for one iteration scales roughly linearly when increasing the number of unknowns from 2229 to 22124, keeping the size of the object compared with the wavelength fixed.

4 Summary of the Publications

The first three papers [P1–P3] treat closed-form solutions of classical electrostatic problems.

In the first paper [P1], we derive the image principle for two orthogonally intersecting conducting spheres using vector calculus and Kelvin’s image principle for a sphere. This classical problem has been considered many times before, but there are still novel aspects in the paper. The derivation is new and the resulting *method of virtual spheres*, which gives a convenient way to find the images of an arbitrary charge distribution, is also new. Furthermore, the relation [P1, Eq. (17)] seems to be new. Also, the novelty of the exact values of the polarizability [P1, Eqs. (45) and (49)] is perhaps small, but the exact values are not easily found in the literature.

The second paper [P2] is again about the electrostatics of two spheres, but this time we consider the non-intersecting case. Using Kelvin’s image principle, it is straightforward to derive the infinite series of images. By solving the corresponding recurrence equations, we get closed-form expressions for the polarizability of the sphere doublet. Although this classical problem has earlier solutions, there are several new aspects of the paper. Again, the derivation is new. In particular, one new idea is to solve the recurrence equations to obtain new expressions for the polarizability. The resulting expression for the transversal polarizability [P2, Eq. (31)] is equivalent with an earlier result, but the expression for the axial polarizability [P2, Eq. (39)] is new. Another novel aspect of the paper is the efficient numerical computation of the polarizability. The quoted 15 digits precision in the transversal polarizability is perhaps massive overkill for most practical purposes, but it is clearly excellent for benchmarking purposes.

In the third paper [P3], we apply Kelvin’s inversion on the image solution for a conducting wedge. We obtain new closed-form solutions for the potential due to a point charge near a conducting object bounded by two intersecting spheres. The solution, using one line image in complex space and a finite number of point images in real space, is efficient also from a purely computational point of view. The line image is smooth and exponentially decaying, and we get an accurate and computationally efficient solution by approximating the line image using a modest number of point images in complex space. There are two

significant novel aspects of the paper. First of all the numerical treatment of the line charge [P3, Sec. 3] and the resulting numerically efficient point-charge approximation are new. Second, the closed form formulas [P3, Eqs. (30)–(32)] are new. The computed examples show that both the exact line image and the point-charge approximation are useful.

The last three papers [P4–P6] are about the fast multipole method (FMM) for electromagnetic and acoustic scattering problems.

In the first of the FMM papers [P4], we consider ways to avoid the sub-wavelength breakdown by using evanescent plane waves in addition to ordinary propagating plane waves. We propose an implementation based on the spectral representation of the Green’s function, and provide some benchmark results for the basic translation procedures. Our approach is different from [45, 49] as we use the samples of the radiation and incoming-wave patterns to represent the fields. This makes the implementation more straightforward, and we can more easily switch to the ordinary (high-frequency) MLFMA for larger cubes. On the other hand, we use different and more efficient quadrature rules than in [48], and also our interpolation procedures are different.

There are several new features in our proposed broadband MLFMA. Both the propagating and evanescent translation procedures are new. Most of the implementation details are based on previously published ideas, but the ideas are developed further and the resulting combination is clearly new. Also the comparison with the UMLFMA [50] is new. The UMLFMA looks promising, but according to our benchmark, its accuracy is poor.

In the last two papers [P5, P6], we apply the broadband MLFMA of [P4] on scattering problems in acoustics and electromagnetics. In both cases, the novel aspect is the combination of a well-conditioned integral equation formulation and a broadband MLFMA solver.

To get a broadband solver, it is not sufficient to only have a broadband MLFMA, but we must also have an integral equation formulation that is well-behaved for all frequencies. In the acoustic case [P5], the formulation is based on the Burton–Miller boundary integral equation, as described in detail in [52]. In the electromagnetic case [P6], we use the well-conditioned Müller formulation that is presented in [25]. In both cases, we show that the proposed combined method avoids the sub-wavelength breakdown.

For the sound-hard plate with holes, using $N = 22124$ unknowns in [P6], we could not solve the problem using a conventional MLFMA. The sparse part of the system matrix would simply have been too large. This particular test case was selected to motivate the need for a broadband MLFMA. In practical problems, a broadband MLFMA could be anything between unnecessary and indispensable depending on the specific geometry and frequency.

The paper [P6] is quite short for two reasons. The used Müller-formulation is described in detail in [23, 25], where the formulation is also compared with other well-conditioned formulations. Therefore, the formulation is just given in [P6] without any further analysis. The second reason is that the fundamen-

tal translation procedures of the broadband MLFMA are given in [P4]. The purpose of [P6] is to show that the combination really gives a broadband solver that avoids the sub-wavelength breakdown in practice. The sphere is a convenient test case, as we know the analytical solution in terms of Mie-series. As such the benchmark only proves with some certainty that the method works for smooth dielectric scatterers with modest dielectric contrast. The surface integral equation formulation has, however, been studied in detail in [23, 25]. In combination with the validations of the broadband MLFMA in [P4–P6], this clearly suggest that the method works also for other dielectric scatterers.

The new broadband MLFMA is usable as implemented in [P5, P6], but there would clearly be room for further improvements. The present implementations are not so well optimized, which results in an unnecessary high memory consumption compared with the theoretical analysis in Section 3.5.2 above. Also the computation times could probably be significantly reduced.

Another potential problem is the error controllability. The errors seems to be slightly worse in practice in [P5, P6] than what is claimed in [P4]. The weakest point is the interpolation and antinterpolation scheme in the complex θ -variable, as described in Section 3.5.1. However, the error-accumulation does not seem to be severe, and for many practical purposes the method should be accurate enough.

Finally, even if the interpolation scheme in the complex θ -variable would need to be replaced, the other parts of the proposed translation procedures are still useful.

References

- [1] W. R. Smythe, *Static and Dynamic Electricity*, 3rd ed. Taylor & Francis, 1989, revised printing.
- [2] J. A. Stratton, *Electromagnetic Theory*. McGraw-Hill, 1941.
- [3] J. D. Jackson, *Classical Electrodynamics*, 3rd ed. Wiley, 1999.
- [4] A. Sihvola, *Electromagnetic mixing formulas and applications*. IEE, 1999.
- [5] J. Avelin, “Polarizability analysis of canonical dielectric and bi-anisotropic scatterers,” Ph.D. dissertation, Helsinki University of Technology, Electromagnetics Laboratory, Report 414, Mar. 2003.
- [6] J. C. Maxwell, *A Treatise on Electricity and Magnetism*, 3rd ed. Clarendon Press, 1891, vol. 1, reprint Dover, 1954.
- [7] W. Thomson (Lord Kelvin), “Extrait d’une lettre de M. William Thomson à M. Liouville,” *Journal de mathématiques pures et appliquées*, vol. 10, pp. 364–367, 1845, also in [9].

- [8] —, “Extraits de deux lettres adressées à M. Liouville,” *Journal de mathématiques pures et appliquées*, vol. 12, pp. 256–264, 1847, also in [9].
- [9] —, *Reprint of Papers on Electrostatics and Magnetism*. London: Macmillan, 1872, ch. XIV.
- [10] O. D. Kellogg, *Foundations of Potential Theory*. J. Springer, 1929, reprint Dover, 1953.
- [11] K. I. Nikoskinen and I. V. Lindell, “Image solution for Poisson’s equation in wedge geometry,” *IEEE Trans. Antennas Propagat.*, vol. 43, no. 2, pp. 179–187, Feb. 1995.
- [12] P. P. Silverster and G. Pelosi, Eds., *Finite Elements for Wave Electromagnetics: Methods and Techniques*. IEEE Press, 1994.
- [13] M. Salazar-Palma, T. K. Sarkar, L.-E. García-Costillo, T. Roy, and A. Djordjević, *Iterative and Self-Adaptive Finite-Elements in Electromagnetic Modeling*. Artech House, 1998.
- [14] J. Jin, *The Finite Element Method in Electromagnetics*, 2nd ed. Wiley, 2002.
- [15] A. Taflové, *Computational Electrodynamics: The Finite-Difference Time-Domain Method*. Artech House, 1995.
- [16] A. Taflové, Ed., *Advances in Computational Electrodynamics: The Finite-Difference Time-Domain Method*. Artech House, 1998.
- [17] R. F. Harrington, *Field Computation by Moment Methods*. Macmillan, 1968.
- [18] E. K. Miller, L. Medgyesi-Mitschang, and E. H. Newman, Eds., *Computational Electromagnetics: Frequency-Domain Method of Moments*. IEEE Press, 1992.
- [19] A. F. Petersen, S. L. Ray, and R. Mittra, *Computational Methods for Electromagnetics*. IEEE Press, 1998.
- [20] B. M. Kolundzija and A. R. Djordjević, *Electromagnetic Modeling of Composite Metallic and Dielectric Structures*. Artech House, 2002.
- [21] S. Järvenpää, M. Taskinen, and P. Ylä-Oijala, “Singularity subtraction technique for high-order polynomial vector basis functions on planar triangles,” *IEEE Trans. Antennas Propagat.*, vol. 54, no. 1, pp. 42–49, Jan. 2006.

- [22] P. Ylä-Oijala, M. Taskinen, and J. Sarvas, “Surface integral equation method for general composite metallic and dielectric structures with junctions,” *Progress in Electromagnetics Research*, vol. PIER 52, pp. 81–108, 2005.
- [23] P. Ylä-Oijala, M. Taskinen, and S. Järvenpää, “Surface integral equation formulations for solving electromagnetic scattering problems with iterative methods,” *Radio Science*, vol. 40, no. 6, Nov. 2005, RS6002.
- [24] M. Taskinen and P. Ylä-Oijala, “Current and charge integral equation formulation,” *IEEE Trans. Antennas Propagat.*, vol. 54, no. 1, pp. 58–67, Jan. 2006.
- [25] P. Ylä-Oijala and M. Taskinen, “Well-conditioned Müller formulation for electromagnetic scattering by dielectric objects,” *IEEE Trans. Antennas Propagat.*, vol. 53, no. 10, pp. 3316–3323, Oct. 2005.
- [26] L. Greengard and V. Rokhlin, “A fast algorithm for particle simulations,” *J. Comput. Phys.*, vol. 73, no. 2, pp. 325–348, Dec. 1987.
- [27] —, “The rapid evaluation of potential fields in three dimensions,” in *Vortex Methods: Proceedings of the U.C.L.A. Workshop Held in Los Angeles, May 20–22, 1987*, ser. Lecture Notes in Mathematics, C. R. Anderson and C. Greengard, Eds., vol. 1360. Springer-Verlag, Dec. 1988, pp. 121–141.
- [28] K. Nabors and J. White, “FastCap: A multipole accelerated 3-D capacitance extraction program,” *IEEE Trans. Computer-Aided Design*, vol. 10, no. 11, pp. 1447–1459, Nov. 1991.
- [29] K. Nabors, S. Kim, and J. White, “Fast capacitance extraction of general three-dimensional structures,” *IEEE Trans. Microwave Theory Tech.*, vol. 40, no. 7, pp. 1496–1506, July 1992.
- [30] V. Rokhlin, “Rapid solution of integral equations of scattering theory in two dimensions,” *J. Comput. Phys.*, vol. 86, no. 2, pp. 414–439, Feb. 1990.
- [31] —, “Diagonal form of translation operators for the Helmholtz equation in three dimensions,” *Appl. Comput. Harm. Anal.*, vol. 1, no. 1, pp. 82–93, Dec. 1993.
- [32] R. Coifman, V. Rokhlin, and S. Wandzura, “The fast multipole method for the wave equation: A pedestrian prescription,” *IEEE Antennas Propagat. Mag.*, vol. 35, no. 3, pp. 7–12, June 1993.
- [33] N. Engheta, W. D. Murphy, V. Rokhlin, and M. S. Vassiliou, “The fast multipole method (FMM) for electromagnetic scattering problems,” *IEEE Trans. Antennas Propagat.*, vol. 40, no. 6, pp. 634–641, June 1992.

- [34] L. R. Hamilton, P. A. Macdonald, M. A. Stalzer, R. S. Turley, J. L. Visher, and S. M. Wandzura, “3D method of moments scattering computations using the fast multipole method,” in *IEEE Antennas and Propagation Society International Symposium*, vol. 1, Seattle, WA, USA, June 1994, pp. 435–438.
- [35] J. M. Song and W. C. Chew, “Fast multipole method solution using parametric geometry,” *Microwave Opt. Tech. Lett.*, vol. 7, no. 16, pp. 760–765, Nov. 1994.
- [36] B. Dembart and E. Yip, “A 3D fast multipole method for electromagnetics with multiple levels,” in *Proceedings 11th Annual Review of Progress in Applied Computational Electromagnetics*, vol. 1, Monterey, CA, USA, Mar. 1995, pp. 621–628.
- [37] J. M. Song and W. C. Chew, “Multilevel fast-multipole algorithm for solving combined field integral equations of electromagnetic scattering,” *Microwave Opt. Tech. Lett.*, vol. 10, no. 1, pp. 14–19, Sept. 1995.
- [38] J. Song, C.-C. Lu, and W. C. Chew, “Multilevel fast multipole algorithm for electromagnetic scattering by large complex objects,” *IEEE Trans. Antennas Propagat.*, vol. 45, no. 10, pp. 1488–1493, Oct. 1997.
- [39] B. Dembart and E. Yip, “The accuracy of fast multipole methods for Maxwell’s equations,” *IEEE Comput. Sci. Eng. Mag.*, vol. 5, no. 3, pp. 48–56, July–Sept. 1998.
- [40] M. F. Guyre and M. A. Stalzer, “A prescription for the multilevel Helmholtz FMM,” *IEEE Comput. Sci. Eng. Mag.*, vol. 5, no. 3, pp. 39–47, July–Sept. 1998.
- [41] M. A. Epton and B. Dembart, “Multipole translation theory for the three-dimensional Laplace and Helmholtz equations,” *SIAM J. Sci. Comput.*, vol. 16, no. 4, pp. 865–987, July 1995.
- [42] J. Rahola, “Diagonal forms of the translation operators in the fast multipole algorithm for scattering problems,” *BIT*, vol. 36, no. 2, pp. 333–358, 1996.
- [43] W. C. Chew, J. M. Jin, E. Michielssen, and J. M. Song, Eds., *Fast and Efficient Algorithms in Computational Electromagnetics*. Artech House, 2001.
- [44] W. C. Chew, H. Y. Chao, T. J. Cui, C. C. Lu, S. Ohnuki, Y. C. Pan, J. M. Song, S. Velampambil, and J. S. Zhao, “Fast integral equation solvers in computational electromagnetics of complex structures,” *Eng. Anal. Bound. Elem.*, vol. 27, no. 8, pp. 803–823, Sept. 2003.

- [45] L. Greengard, J. Huang, V. Rokhlin, and S. Wandzura, “Accelerating fast multipole methods for the Helmholtz equation at low frequencies,” *IEEE Comput. Sci. Eng. Mag.*, vol. 5, no. 3, pp. 32–38, Jul.–Sep. 1998.
- [46] J.-S. Zhao and W. C. Chew, “Three-dimensional multilevel fast multipole algorithm from static to electrodynamic,” *Microwave Opt. Tech. Lett.*, vol. 26, no. 1, pp. 43–48, July 2000.
- [47] L. J. Jiang and W. C. Chew, “A mixed-form fast multipole algorithm,” *IEEE Trans. Antennas Propagat.*, vol. 53, no. 12, pp. 4145–4156, Dec. 2005.
- [48] ———, “Low-frequency fast inhomogeneous plane-wave algorithm (LF-FIPWA),” *Microwave Opt. Tech. Lett.*, vol. 40, no. 2, pp. 117–122, Jan. 2004.
- [49] E. Darve and P. Havé, “A fast multipole method for Maxwell equations stable at all frequencies,” *Phil. Trans. R. Soc. Lond. A*, vol. 362, no. 1816, pp. 603–628, Mar. 2004.
- [50] L. Xuan, A. Zhu, R. J. Adams, and S. D. Gedney, “A broadband multilevel fast multipole algorithm,” in *IEEE AP-S International Symposium and USNC/URSI National Radio Science Meeting*, vol. 2, Monterey, CA, USA, June 2004, pp. 1195–1198.
- [51] J. Sarvas, “Performing interpolation and antepolation entirely by fast fourier transform in the 3-D multilevel fast multipole algorithm,” *SIAM J. Numer. Anal.*, vol. 41, no. 6, pp. 2180–2196, 2003.
- [52] P. Ylä-Oijala and S. Järvenpää, “Iterative solution of high-order boundary element method for acoustic impedance boundary value problems,” *J. Sound Vibr.*, vol. 291, no. 3–5, pp. 824–843, Apr. 2006.